FLOW AND HEAT-TRANSFER MODELLING OF THREE-DIMENSIONAL JET IMPINGEMENT ON A CONCAVE SURFACE

Tim J. Craft, Hector Iacovides, Nor A. Mostafa
School of Mechanical, Aerospace & Civil Engineering,
The University of Manchester,
Manchester M60 1QD, UK
tim.craft@manchester.ac.uk

ABSTRACT

The paper reports computations of the flow and heat-transfer from a round jet impinging onto a concave semi-circular surface, designed to reproduce important flow features found in internal turbine blade cooling applications. Linear and non-linear eddy-viscosity models are applied, with wall-functions to cover the near-wall layer, and are shown to capture the overall flow characteristics. The standard, log-law based, form of wall-function is found to be inadequate in predicting the heat-transfer, and a more advanced form developed at Manchester (the AWF) is also tested. The exact way in which convective terms are approximated in this latter approach is shown to be crucial, and a form is presented which leads to stable and reasonably accurate solutions.

INTRODUCTION

To achieve efficient cooling of blades within a modern gas turbine, internal blade cooling passages are typically employed. The complex geometrical shape of these results in many flow features being present, including separation, reattachment, strong secondary flows and impingement, in addition to system rotation.

There have been many studies, both experimental and computational, of the effects of sharp U-turns and the rib-rougheners that are typically employed in cooling passages to enhance heat-transfer. A recent review is presented in Launder & Iacovides (2006). Other, equally important, features, such as impingement cooling, have received some attention, (Mattern & Hennecke, 1996; Akella & Han, 1998, for example), but have not been so widely studied in the context of blade cooling. Whilst there are numerous studies of jet impingement onto flat plates, few have considered impingement onto the type of curved surfaces found within blade cooling passages. Fewer still have studied such flows under the rotating conditions found in blade applications.

Advances in the availability of computing resources mean that it is now feasible to perform numerically accurate simulations of the flow and heat-transfer through internal cooling passages. However, in order to obtain physically accurate results the models of turbulence employed must be capable of correctly representing the diverse and challenging flow features referred to above. The most widely used linear eddy-viscosity schemes are known to fail in many complex flows, including those involving separation and impingement. Full stress transport models have a better physical basis, but are more computationally expensive. As a result, non-linear eddy-viscosity models have received significant interest in recent years, as they have been seen to offer the promise of considerable predictive improvements over linear schemes with only a modest increase in cost. A further consideration in the modelling of these flows is the handling of the near-wall viscosity-affected layer. Whilst the most accurate method is to employ a fine near-wall grid with a turbulence model containing low-Reynolds-number and appropriate near-wall terms, the requirement to resolve this layer fully leads to very high computational costs. Gant (2002), for example, reported an order of magnitude difference in required cpu time between low-Reynolds-number and wall-function approaches. As a result, wall-function approaches are widely employed for such industrial applications. However, the standard forms adopted are known to give an inaccurate representation of the near-wall flow in most complex flow situations, and so the present work has tested an alternative, more widely applicable, formulation developed by the Manchester group.

The present contribution focuses on the prediction of jet impingement onto a concave surface: a situation typically employed for the internal cooling of the leading edge of a blade, as shown in Figure 1. Detailed measurements of a relevant flow have been reported by Iacovides et al. (2005), using an array of jets impinging onto the curved wall of a semi-circular passage, as shown in Figure 2. This arrangement contains many of the important physical features found in such cooling applications, but is a simple enough geometry, with well-defined boundary conditions, to allow a detailed and informative comparison of computed and measured velocities, stresses and heat-transfer to be made.

The sections below give details of the case studied, the modelling and numerical approaches adopted, and present a comparison between the results obtained with different modelling strategies and the measured data.

CASE STUDIED

The case studied experimentally by Iacovides et al. (2005) consisted of a row of five circular jets impinging onto the heated concave surface of a semi-circular passage (see Figure 2). Heat-transfer measurements were made on the concave surface, as well as mean velocity and turbulence mea-

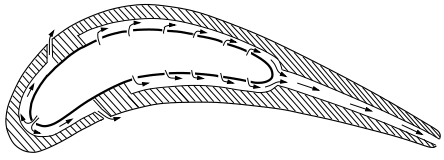

Figure 1: Impingement cooling in the leading edge of a turbine blade.

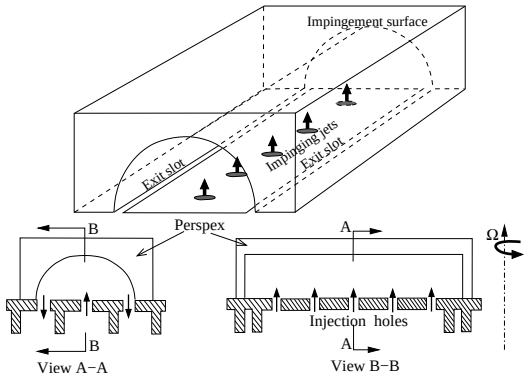

Figure 2: Geometry of Iacovides et al. (2005)

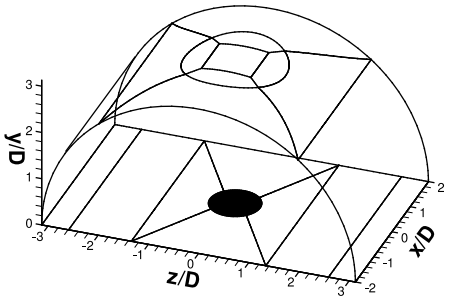

Figure 3: Computational domain.

surements on a number of planes across the passage. The Reynolds number, based on inlet jet velocity and diameter, was 9,400 for the velocity field measurements and 15,000 for the heat-transfer. The whole assembly could be rotated about an axis parallel to that of the jets, in order to study the effect of system rotation. However, simulations reported here are only of non-rotating cases.

To reduce computational costs, the present calculations have considered the flow around a single jet, on a domain shown in Figure 3, with symmetry conditions applied on the planes $x/D = \pm 2$. The circular jet enters the domain at the centre of the x-z plane, impinges onto the semi-circular outer wall at a height of three jet diameters above the inlet, and the fluid exits the domain via channels half a jet diameter wide, running along the two edges of the base-plane parallel to the x-axis. The simulation results have been compared to measurements of the central jet shown in Figure 2.

TURBULENCE MODELLING

Fully Turbulent Flow Region

Linear eddy-viscosity models are not expected to capture accurately many of the flow features found in the present complex application. Whilst calculations have, nevertheless, been performed with a linear k-ε model for comparison purposes, the main emphasis in the present study has thus been on the use of non-linear eddy-viscosity models, which have been shown in a number of cases to return results much superior to linear schemes, for only a modest increase in computational cost (see Craft et al. (1996), for example). In this work the model variant detailed by Craft et al. (1999) has been employed, which is a development of the cubic model originally devised by Suga (1995), and has been shown to perform well in a range of flows.

The linear k-ε model solves transport equations for k and ε of the form

$$\frac{Dk}{Dt} = P_k - \varepsilon + \frac{\partial}{\partial x_k}\left(\frac{\nu_t}{\sigma_k}\frac{\partial k}{\partial x_k}\right) \quad (1)$$

$$\frac{D\varepsilon}{Dt} = c_{\varepsilon 1}\frac{\varepsilon P_k}{k} - c_{\varepsilon 2}\frac{\varepsilon^2}{k} + \frac{\partial}{\partial x_k}\left(\frac{\nu_t}{\sigma_\varepsilon}\frac{\partial \varepsilon}{\partial x_k}\right) \quad (2)$$

and approximates the Reynolds stresses by

$$\overline{u_i u_j} = (2/3)k\delta_{ij} - \nu_t\left(\partial U_i/\partial x_j + \partial U_j/\partial x_i\right) \quad (3)$$

with $\nu_t = c_\mu k^2/\varepsilon$ and model coefficients given in Table 1.

The non-linear model employed here retains essentially the same transport equations for k and ε, but uses a non-linear relation for the Reynolds stresses:

$$\begin{aligned}\overline{u_i u_j} = {} & \tfrac{2}{3}k\delta_{ij} - \nu_t S_{ij} + c_1\frac{\nu_t k}{\varepsilon}\left(S_{ik}S_{kj} - \tfrac{1}{3}S_{kl}S_{kl}\delta_{ij}\right) \\ & + c_2\frac{\nu_t k}{\varepsilon}\left(\Omega_{ik}S_{kj} + \Omega_{jk}S_{ki}\right) \\ & + c_3\frac{\nu_t k}{\varepsilon}\left(\Omega_{ik}\Omega_{jk} - \tfrac{1}{3}\Omega_{lk}\Omega_{lk}\delta_{ij}\right) \\ & + c_4\frac{\nu_t k^2}{\varepsilon^2}\left(S_{ki}\Omega_{lj} + S_{kj}\Omega_{li}\right)S_{kl} \\ & + c_6\frac{\nu_t k^2}{\varepsilon^2}S_{ij}S_{kl}S_{kl} + c_7\frac{\nu_t k^2}{\varepsilon^2}S_{ij}\Omega_{kl}\Omega_{kl} \end{aligned} \quad (4)$$

where the mean strain and vorticity tensors are defined by $S_{ij} = \partial U_i/\partial x_j + \partial U_j/\partial x_i$ and $\Omega_{ij} = \partial U_i/\partial x_j - \partial U_j/\partial x_i$.

The turbulent viscosity is again taken as $\nu_t = c_\mu k^2/\varepsilon$, but c_μ is now given by the expression

$$c_\mu = \min\left[0.09, \frac{1.2}{1 + 3.5\eta + f_{RS}}\right] \quad (5)$$

with $f_{RS} = 0.235(\max(0, \eta - 3.333))^2\sqrt{S_I^2}$ and

$$\eta = (k/\varepsilon)\max\left\{\sqrt{S_{ij}S_{ij}/2}, \sqrt{\Omega_{ij}\Omega_{ij}/2}\right\} \quad (6)$$

$$S_I = S_{ij}S_{jk}S_{ki}/\left(S_{nl}S_{nl}/2\right)^{3/2} \quad (7)$$

Other coefficients are given in Table 1.

As implemented in the computer code, both the above models contain additional low-Reynolds-number and near-wall terms, as detailed in Launder & Sharma (1974) and Craft et al. (1999) respectively. However, with the grid employed in the present calculations, the near-wall viscosity-affected layer is accounted for by the use of wall-functions. The low-Reynolds-number terms in the models thus have a negligible effect and, for clarity, are not described here.

Table 1: Model coefficients in the linear and non-linear k-ε models.

$c_{\varepsilon 1}$	$c_{\varepsilon 2}$	σ_k	σ_ε
1.44	1.92	1.0	1.22

Linear	Non-linear					
c_μ	c_1	c_2	c_3	c_4	c_6	c_7
0.09	-0.1	0.1	0.26	$-10c_\mu^2$	$-5c_\mu^2$	$5c_\mu^2$

Near-Wall Modelling

One significant problem in 3-D cases such as the present is the handling of the near-wall, viscosity-affected layer. A full resolution of this, with a low-Reynolds-number turbulence model, is very expensive, as a result of the extremely fine grid needed. Hence the present work has used wall-functions to approximate the flow development across this layer, allowing

the use of a coarser near-wall grid, with the first near-wall node ideally placed outside the viscous layer, in the fully-turbulent region of the flow.

Standard forms of wall-functions are based on an assumed logarithmic mean velocity profile and local equilibrium conditions, leading to the near-wall velocity and temperature profiles being given in non-dimensional form as

$$U^* = (1/\kappa^*)\log(E^* y^*) \quad T^* = \sigma_t[U^* + P^*(\sigma/\sigma_t)] \quad (8)$$

where $U^* = U k_p^{1/2}/\tau_w$, $T^* = (T_w - T)\rho C_p k_p^{1/2}/\dot{q}_w$, and $y^* = y k_p^{1/2}/\nu$ with τ_w the wall shear stress, $\dot{q}_w$ the wall heat flux, T_w the wall temperature, σ and σ_t the molecular and turbulent Prandtl numbers, y the distance from the wall, k_p the turbulent kinetic energy at the near-wall node, κ^* and E^* constants and P^* the Jayatilleke (1969) pee-function.

However, the above conditions are known to not hold in many situations (including the complex near-wall flow field of the present case). In recent work at Manchester, Craft et al. (2002) developed an improved wall-function approach (the analytic wall-function, or AWF), designed to be more widely applicable. In this approach the assumption is made that the turbulent viscosity increases linearly from the edge of the viscous sublayer, y_v (defined by $y_v^* = 10.8$), to the outer edge of the near wall cell, y_n:

$$\mu_t = \begin{cases} 0 & \text{for } 0 < y < y_v \\ \mu c_l c_\mu (y^* - y_v^*) & \text{for } y_v < y < y_n \end{cases} \quad (9)$$

with constants $c_l = 2.55$, $c_\mu = 0.09$. One can then write the near-wall mean temperature equation in the simplified form

$$\frac{\partial}{\partial y}\left[\frac{\mu}{\sigma}\frac{\partial T}{\partial y}\right] = C_{th1} \quad \text{for } 0 < y < y_v$$

$$\frac{\partial}{\partial y}\left[\mu\left[\frac{1}{\sigma} + \frac{c_l c_\mu}{\sigma_t}(y^* - y_v^*)\right]\frac{\partial T}{\partial y}\right] = C_{th2} \quad \text{for } y_v < y < y_n \quad (10)$$

where C_{th1} and C_{th2} represent the convective transport terms in the two layers of the cell. If these are assumed constant across each layer, the above equations can be integrated analytically, applying boundary conditions that $T = T_n$ at the outer edge of the cell (see Figure 4), that T and $\partial T/\partial y$ are continuous at $y = y_v$ and that either the temperature or heat flux are known at the wall. The result is an analytic expression for the temperature across the near-wall cell, which can be used to set the computational boundary conditions within a wall-function approach. A similar treatment can be applied to the wall-parallel momentum equation, where convective and pressure gradient terms now appear in the corresponding expressions to the right hand sides of equation (10). Full details of the derivations and forms employed, and examples of applications, can be found in Craft et al. (2002) and Gerasimov (2003).

A crucial element in applying the AWF to the present problem is the approximation of the convective terms C_{th1} and C_{th2} in the simplified temperature equation. In the applications referred to above only the convective transport tangential to the wall surface, C_{tht}, was retained, which was simply evaluated in terms of nodal values:

$$C_{th1} = C_{th2} = \underbrace{\rho U \frac{\partial T}{\partial x}}_{C_{tht}} + \underbrace{\rho V \frac{\partial T}{\partial y}}_{C_{thn}} \approx \rho U_P\left[\frac{T_e - T_w}{\Delta x}\right] \quad (11)$$

where quantities at the cell faces e and w were evaluated by interpolating between nodal values at P, E, W as indicated in Figure 4. However, the applications considered did not include strongly impinging flows such as the present one, and in this case the wall-normal convection, C_{thn}, and the exact form adopted to represent it, become crucially important. An initial approach tested was to approximate the wall-normal convection in terms of nodal values, in a manner similar to that for the tangential convection, so

$$C_{th1} = C_{th2} = \rho U_P\left(\frac{T_e - T_w}{\Delta x}\right) + \rho V_P\left(\frac{T_n - T_{wall}}{\Delta y}\right) \quad (12)$$

However, since most of the temperature variation occurs across the thin viscosity-affected layer, the above approximation is far from accurate, and results in a significant overprediction of the stagnation heat-transfer. Instead, therefore, the approach outlined below has been adopted.

The convection contributions C_{th1} and C_{th2} are approximated by obtaining "average" values for $U\,\partial T/\partial x$ and $V\,\partial T/\partial y$ across the two layers $0 < y < y_v$ and $y_v < y < y_n$ respectively:

$$C_{th1} = \frac{1}{y_v}\int_0^{y_v} \rho\left[U(\partial T/\partial x) + V(\partial T/\partial y)\right] dy \quad (13)$$

$$C_{th2} = \frac{1}{(y_n - y_v)}\int_{y_v}^{y_n} \rho\left[U(\partial T/\partial x) + V(\partial T/\partial y)\right] dy \quad (14)$$

The integrals are evaluated using the analytical profiles for U and $\partial T/\partial y$; approximating the wall-parallel gradient as $\partial T/\partial x \approx (T_e - T_w)/\Delta x$, and taking an assumed variation for the wall-normal velocity V across the cell. After testing a number of alternatives, the form adopted for the variation of V was a quadratic increase across the sublayer $0 < y < y_v$, followed by a piecewise linear variation through V_P and V_n, as shown in Figure 4. An entirely analoguous treatment has also been applied to the convection terms in the simplified momentum equation (see Mostafa (2007) for details).

Whilst the above treatment performed satisfactorily in the impingement region, the inclusion of wall-normal convection in the temperature equation in areas where the near-wall flow was directed away from the wall resulted in the predicted wall temperature becoming very large in magnitude, leading to numerical convergence problems. This unwanted behaviour was traced to a feedback mechanism in the resulting algebraic expression for the temperature gradient, $\partial T/\partial y$, when it is negative and wall-normal convection (which depends on $\partial T/\partial y$) is included. To prevent this, the above wall-normal convection contribution is only included in the temperature equation when the near-wall flow is directed towards the wall, and is neglected if the flow is away from the wall. This treatment allowed fully converged solutions to be obtained for both the momentum and temperature equations.

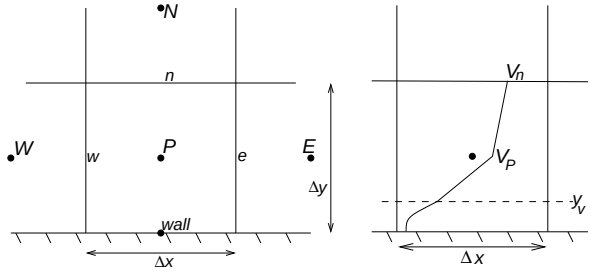

Figure 4: AWF near-wall grid arrangement and assumed wall-normal velocity variation.

NUMERICAL TREATMENT

The simulations have been performed using a modified version of the STREAM code (Lien & Leschziner, 1994), which is a finite volume solver employing the SIMPLE pressure correction scheme with Rhie & Chow (1983) interpolation used to avoid chequerboarding arising from the fully collocated grid storage arrangement. The UMIST convection scheme (Leschziner & Lien, 1994) was employed for mean variables, with first order upwind applied for turbulence quantities.

Structured multi-block grids were generated, and Figure 5 shows details of a typical such grid. Most calculations have been performed on a grid with approximately a quarter of a million cells, with typical near-wall nodes being at a non-dimensional distance of around $y^* \approx 40$ from the wall. Grid refinement tests using a finer grid of around one million cells were found to give almost identical results to those obtained on the coarser mesh with, for example, the peak Nusselt number predictions differing by less than 2%. Hence, for computational efficiency, most of the results reported here have been obtained on the coarser mesh.

The jet inlet conditions were modelled by applying a constant velocity, turbulence intensity of 15% and viscosity ratio ν_t/ν of 50 across the inlet, except for a band of width $0.2D$ around the outer edge of the jet, where a power-law was fitted to the velocity profile and a mixing-length approximation used to evaluate turbulence levels. This approach helps to form the mixing layer development between the jet and surrounding fluid, and has been tuned in the present case to match available measurements close to the jet inlet.

Symmetry conditions were applied on the planes at $x/D = \pm 2$, and zero-gradient conditions on all variables at the outlet channels. All other boundaries were walls, treated with the wall-function approaches described above.

RESULTS

Figure 6 shows measured and predicted velocity vectors on the mid-depth plane $x = 0$. Computed results are shown for the linear model with standard wall-functions, although those obtained with other model combinations are almost indistinguishable from these. As shown in the figure, the jet impinges on the curved surface, resulting in a wall jet developing along this surface. On the planes $x/D = \pm 2$ this wall jet collides with those developing from the adjacent jets, resulting in the downwash shown in the vector plots on the $z = 0$ plane in Figure 7. As a result of these interactions there is a complex flow circulation pattern. As can be seen in Figure 6, the simulations indicate that on the $x = 0$ plane there is a significant region of the curved surface (from around $z/D = 2.4$ to just above the exit channel) where the near-wall flow is vertically upwards. The figures show that these predicted flow features do broadly reproduce the behaviour seen in the measurements.

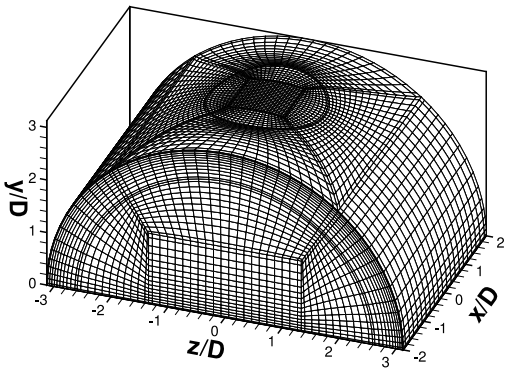

Figure 5: Details of computational grid.

Figure 8 shows profiles of the vertical velocity at several locations on the plane $x = 0$. The choice of which wall-function is employed has little effect on these profiles so, for clarity, only results employing the standard wall-function are shown. Figure 9 shows corresponding profiles of the rms v' component. Both models produce very similar mean velocity profiles, in general accord with the data, and although the non-linear scheme returns higher streamwise stress levels in the jet mixing layer, both models predict significantly lower turbulence levels than those measured as one moves away from the jet inlet. These lower turbulence levels can be expected to result in the overpredicted peak V levels seen at $y/D = 2.23$ and 2.86 in Figure 8.

Whilst the velocity and stress profiles shown above are not particularly sensitive to the wall treatment adopted, the heat-transfer is strongly affected by the choice of wall-function. Figure 10 shows the predicted Nusselt number distribution on the curved surface for the linear and non-linear models using the standard wall-function, compared to the measurements of Iacovides et al. (2005). As can be seen, the peak levels predicted in the jet impingement region are rather lower than the

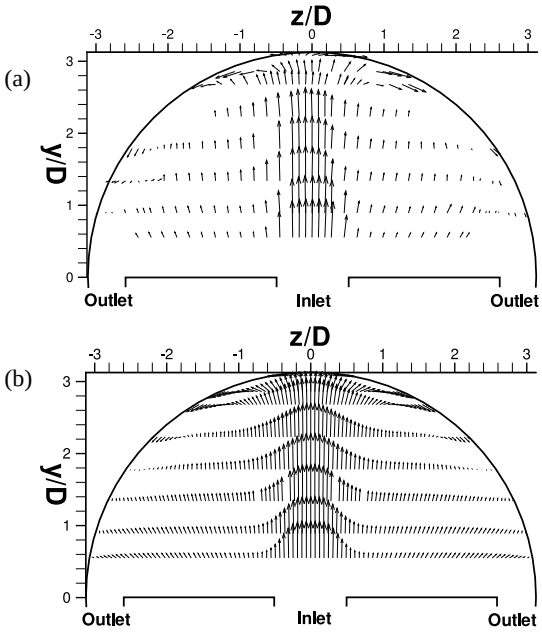

Figure 6: Measured (a) and computed (b) velocity vectors on the plane $x = 0$.

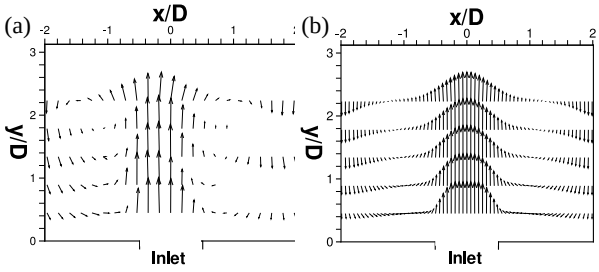

Figure 7: Measured (a) and computed (b) velocity vectors on the plane $z = 0$.

measurements. The secondary peaks, shown in the measurements on the centreline at $x/D = \pm 2$ where the jet downwash occurs, are also not captured by the computations.

A more quantitative comparison is seen in Figure 11 which shows profiles of the predicted and measured Nusselt number along the line $z/D = 0$ (the top of the curved surface). As noted in the contour plots, both model combinations underpredict the peak Nusselt number and return profiles which decrease continuously from the centre to the edges at $x/D = \pm 2$, whilst the measured data show a flatter profile in the outer regions, with small secondary peaks at $x/D = \pm 2$.

Although Figure 11 suggests the linear EVM gives a better estimate of the peak heat-transfer level than the non-linear scheme, the latter is known to produce a generally more reliable representation of the dynamic field in many complex flows, and it is therefore this model that has been tested in combination with the AWF near-wall treatment. The resulting heat-transfer predictions from applying the AWF, as described in the modelling section above, with the non-linear EVM are shown in Figures 12 and 13. As can be seen the peak heat-transfer is now slightly underpredicted, but shows a fairly flat profile across the peak, in reasonable agreement with the measurements. Initial computations of the full five jet geometry suggest that slightly asymmetric interactions between the jets result in a small increase of peak heat transfer levels, bringing them into close agreement with the data. At the outer edge of the domain, for $|x/D| > 1.5$, the levels of Nu are underpredicted, although the simulations do show clear secondary peaks as suggested by the experimental data.

As noted earlier, the heat-transfer predictions in this flow are rather sensitive to the approximation employed for the convective transport in the wall-function, particularly the wall-normal convection C_{thn}. To underline this, although not shown here, if the contribution from C_{thn} is neglected entirely, the AWF results show an underpredicted maximum Nusselt number of around 180, whilst if a simple approxima-

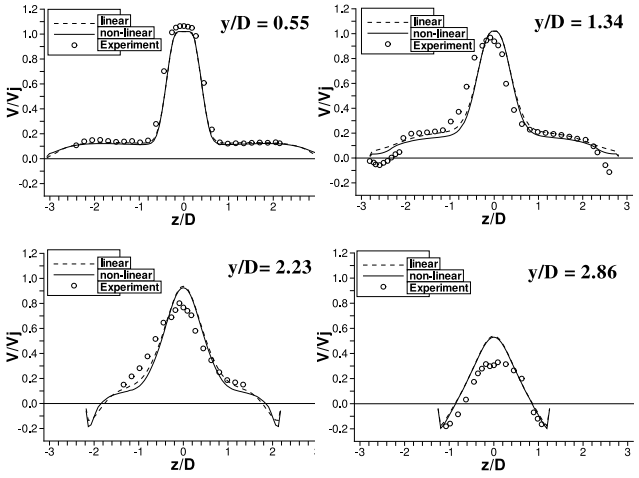

Figure 8: Profiles of vertical velocity on the plane $x = 0$ at four y/D positions. Inlet jet covers the region $|z/D| < 0.5$. ——: Non-linear EVM; - - : Linear EVM; Symbs.: Expts. of Iacovides et al. (2005).

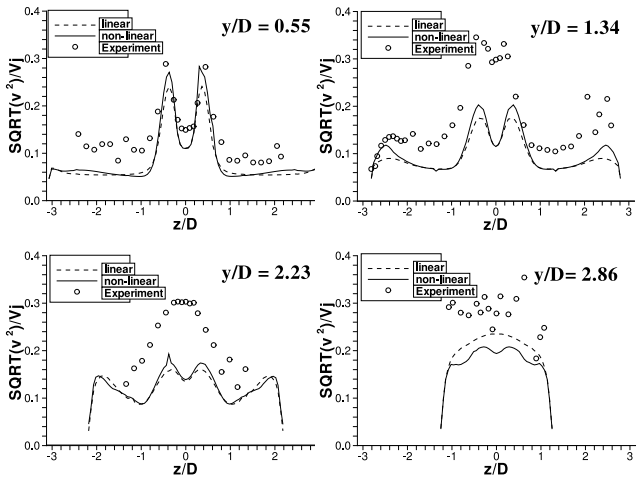

Figure 9: Reynolds stress profiles on the plane $x = 0$ at four y/D positions. Key as in Figure 8

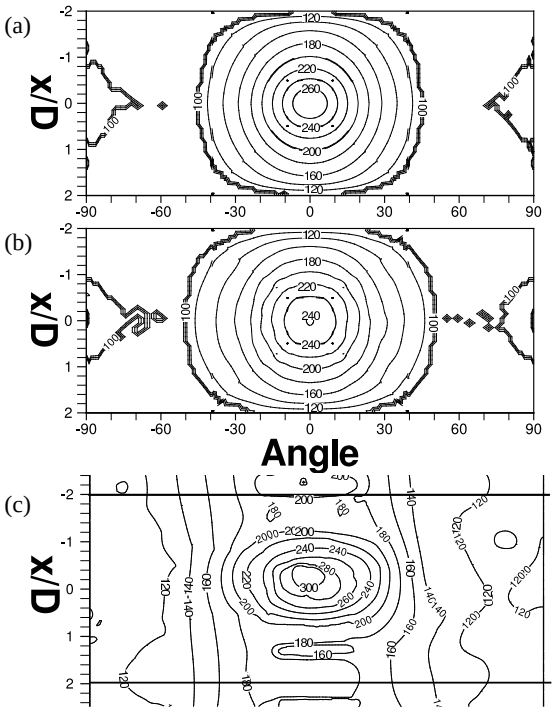

Figure 10: Nusselt number on the curved surface computed with standard wall-functions. (a) Linear k-ε; (b) Non-linear k-ε; (c) Expts. of Iacovides et al. (2005).

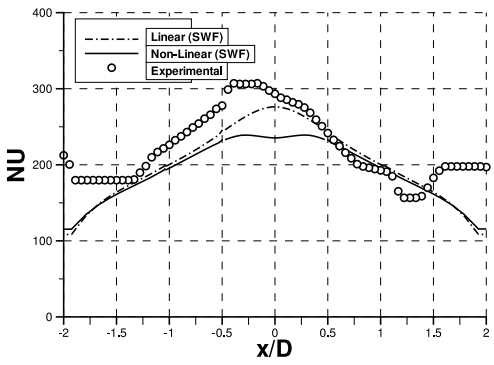

Figure 11: Nusselt number profiles on the curved surface along the line $z/D = 0$. Predictions using standard wall-functions; Expts. of Iacovides et al. (2005).

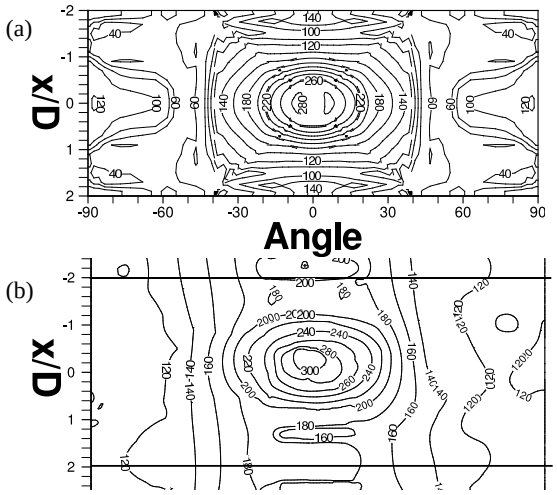

Figure 12: Nusselt number contours using the non-linear EVM and AWF with proposed convection model. (a) calculations; (b) Expts. of Iacovides et al. (2005).

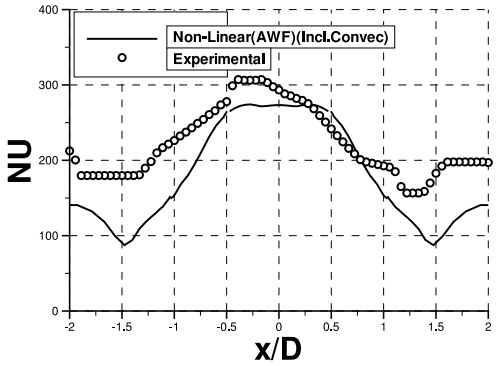

Figure 13: Nusselt number profiles on the curved surface along the line $z/D = 0$. Predictions using non-linear EVM and AWF; Expts. of Iacovides et al. (2005).

tion based on nodal values, as in equation (12), is adopted the predicted peak Nusselt number is around 700.

CONCLUSION

When applied to the present configuration, both the linear and non-linear eddy-viscosity schemes broadly reproduce the mean flow field. Although the non-linear model produces the slightly better turbulence stress levels, both schemes appear to underpredict the levels of turbulence energy as the jet approaches the curved surface.

The use of standard wall-functions results in underpredicted heat-transfer levels around the jet impingement, and a failure to capture the secondary Nusselt number peaks associated with the jet downwash. The AWF results are highly sensitive to the the approximation adopted to represent wall-normal convective transport in this impingement-domianted flow. The proposed form was found to be numerically stable and to give broadly the correct peak Nu number levels, together with secondary peaks associated with the jet downwash, although the overall heat transfer levels are somewhat underpredicted in this region of the flow.

Subsequent studies are currently under way to simulate the full five-jet geometry studied in the experiments, under both stationary and rotating conditions.

ACKNOWLEDGEMENTS

The research has been supported by Tenaga Nasional Berhad, Malaysia.

REFERENCES

Akella, K., Han, J.-C. (1998), "Impingement cooling in rotating two-pass rectangular channels", *J. of Thermophysics & Heat Transfer*, **12**, 582–588.

Craft, T. J., Gerasimov, A. V., Iacovides, H., Launder, B. E. (2002), "Progress in the generalization of wall-function treatments", *Int. J. Heat Fluid Flow*, **23**, 148–160.

Craft, T. J., Iacovides, H., Yoon, J. H. (1999), "Progress in the use of non-linear two-equation models in the computation of convective heat-transfer in impinging and separated flows", *Flow, Turbulence and Combustion*, **63**, 59–80.

Craft, T. J., Launder, B. E., Suga, K. (1996), "Development and application of a cubic eddy-viscosity model of turbulence", *Int. J. Heat and Fluid Flow*, **17**, 108–115.

Gant, S. E. (2002), "Development and application of a new wall function for complex turbulent flows", Ph.D. thesis, Department of Mechanical, Aerospace & Manufacturing Engineering, UMIST, Manchester.

Gerasimov, A. V. (2003), "Development and application of an analytical wall-function strategy for modelling forced, mixed and natural convection flows", Ph.D. thesis, Department of Mechanical, Aerospace & Manufacturing Engineering, UMIST, Manchester.

Iacovides, H., Kounadis, D., Launder, B. E., Li, J.-K., Xu, Z.-Y. (2005), "Experimental study of the flow and thermal development of a row of cooling jets impinging on a rotating concave surface", *ASME J. Turbomachinery*, **127**, 222–229.

Jayatilleke, C. L. V. (1969), "The influence of Prandtl number and surface roughness on the resistance of the laminar sublayer to momentum and heat transfer", *Prog. Heat Mass Transfer*, **1**, 193.

Launder, B. E., Iacovides, H. (2006), "Internal blade cooling: the Cinderella of turbomachinery C&EFD", in Proc. 12th Int. Heat Transfer Conference, Sydney.

Launder, B. E., Sharma, B. I. (1974), "Application of the energy-dissipation model of turbulence to the calculation of flow near a spinning disc", *Lett. in Heat Mass Transfer*, **1**, 131–138.

Leschziner, M. A., Lien, F. S. (1994), "Upstream monotonic interpolation for scalar transport with application to complex turbulent flows", *Int. J. for Numerical Methods in Fluids*, **19**, 527–548.

Lien, F.-S., Leschziner, M. A. (1994), "A general non-orthogonal finite-volume algorithm for turbulent flow at all speeds incorporating second-moment turbulence-transport closure", *Comp. Meth. Appl. Mech. Eng.*, **114**, 123–167.

Mattern, C., Hennecke, D. (1996), "The influence of rotation on impingement cooling", in ASME Paper 96-GT-161, Int. Gas Turbine and Aero Congress, Birmingham, UK.

Mostafa, N. (2007), "Computational studies of blade cooling related turbulent flows", Ph.D. thesis, University of Manchester.

Rhie, C. M., Chow, W. L. (1983), "Numerical study of the turbulent flow past an airfoil with trailing edge separation", *AIAA J.*, **21**, 1525–1532.

Suga, K. (1995), "Development and application of a non-linear eddy viscosity model sensitized to stress and strain invariants", Ph.D. thesis, Faculty of Technology, University of Manchester.